The crystal structure of charmarite – the first case of a 11 × 11 Å superstructure mesh in layered double hydroxides

Elena S. Zhitova[1]*, Andrey A. Zolotarev[1,2], Anatoly V. Kasatkin[3], Rezeda M. Sheveleva[1,2], Sergey V. Krivovichev[2,4], Igor V. Pekov[5], Vladimir N. Bocharov[2]

Short title: crystal structure of charmarite: new type of ordering

[1] Institute of Volcanology and Seismology, Russian Academy of Sciences, Bulvar Piipa 9, 683006 Petropavlovsk-Kamchatsky, Russia

[2] St. Petersburg State University, University Emb. 7/9, 199034 St. Petersburg, Russia

[3] Fersman Mineralogical Museum, Russian Academy of Science, Leninskiy Prospect 18-2, 119071 Moscow, Russia

[4] Nanomaterials Research Centre, Kola Science Centre, Russian Academy of Sciences, Fersman Street 14, 184209 Apatity, Russia

[5] Faculty of Geology, Moscow State University, Leninskie Gory 1, 119991 Moscow, Russia

Corresponding author: Elena Zhitova zhitova_es@mail.ru

Abstract

Charmarite, $Mn_4Al_2(OH)_{12}CO_3 \cdot 3H_2O$, is a hydrotalcite supergroup member (or layered double hydroxide, LDH) with previously unknown crystal structure and a Mn^{2+}-analogue of quintinite (commonly erroneously reported as "2:1 hydrotalcite"). The single-crystal X-ray diffraction (XRD) data were obtained from the specimen from Mont Saint-Hilaire, Québec, Canada and are best processed in the space group P-3, a = 10.9630(4), c = 15.0732(5) Å, V = 1568.89(12) Å^3. The crystal structure has been solved by direct methods and refined to R_1 = 0.0750 for 3801 unique reflections with $F_o > 4\sigma(F_o)$. The charmarite structure has the long-range periodicity in

This is a 'preproof' accepted article for Mineralogical Magazine. This version may be subject to change during the production process.
DOI: 10.1180/mgm.2024.11

the *xy* plane due to $2\sqrt{3}a' \times 2\sqrt{3}a'$ scheme (or 11 × 11 Å) determined for LDHs for the first time (where a' is a subcell parameter ~ 3.2 Å). This periodicity is produced by the combination of two superstructures formed by: (i) Mn^{2+} and Al^{3+} ordering in the metal-hydroxide layers $[Mn_4Al_2(OH)_{12}]^{2+}$ according to the $\sqrt{3}a' \times \sqrt{3}a'$ pattern and (ii) the $(CO_3)^{2-}$ ordering according to the $2a' \times 2a'$ pattern in the $[CO_3(H_2O)_3]^{2-}$ interlayer sheet in order to avoid close contacts between adjacent carbonate groups. The $2\sqrt{3}a' \times 2\sqrt{3}a'$ superstructure is an example of the adaptability of the components of the interlayer space to the charge distribution of the metal-hydroxyl layers. The Mn^{2+} and Al^{3+} cations have large difference in size, which apparently leads to the considerable degree of their order as di- and trivalent cations resulting in a higher degree of statistical order of the interlayer components. Both powder and single-crystal XRD data show that studied samples belong to the hexagonal branch of two-layer polytypes (2*T* or 2*H*) with d_{00n} ~ 7.57 Å. The chemical composition of the studied samples is close to the ideal formula. The Raman spectrum of charmarite is reported and the band assignment is provided.

Keywords: charmarite; quintinite; hydrotalcite; layered double hydroxide; natural LDH; crystal structure; Mont Saint-Hilaire alkaline complex

Introduction

Charmarite, ideally $Mn_4Al_2(OH)_{12}CO_3 \cdot 3H_2O$, is a member of the quintinite group (with the ratio between di- and trivalent cations equal to $M^{2+}:M^{3+} = 2:1$), which is a part of the hydrotalcite supergroup (Mills *et al.*, 2012), a natural branch of the layered double hydroxide (LDH) family (Rives, 2001; Evans and Slade, 2006). Layered double hydroxides are united by a common structural motif in which brucite-like metal-hydroxyl layers (or octahedral sheets) formed by di- and trivalent (in specific cases also monovalent) metals and interlayers alternate (Rives, 2001). The positive charge of the brucite-like metal-hydroxide layers is compensated by the negatively charged interlayer species. In some cases, metal-hydroxide layers are gibbsite-based (formed primarily by trivalent cations), where monovalent cations [or divalent cations as shown by synthetic materials (Andersen *et al.*, 2021)] produce positive charge of the layers (Serna *et al.*, 1982; Sissoko *et al.*, 1985; Britto and Kamath, 2011; Karpenko *et al.*, 2020). Layered double hydroxides are used in catalytic (Karim *et al.*, 2022; Xu and Wei, 2018; Bosa *et al.*, 2023) and pharmaceutical (Guilherme *et al.*, 2022) applications, are of interest from the material science point of view as sorbents and ion exchangers (Forano *et al.*, 2006), and are useful for the design of new materials (Sotiles and Wypych, 2019). Synthetic analogue of

https://doi.org/10.1180/mgm.2024.11 Published online by Cambridge University Press

charmarite can be obtained by co-precipitation and may be of interest for catalytic applications (Grand *et al.*, 2010).

Charmarite was first described in well-shaped hexagonal crystals from the Mont Saint-Hilaire alkaline complex, Québec, Canada in two polytypic modifications, 2*H* and 3*T* (Chao and Gault, 1997). In the cited paper, charmarite was described together with two other new minerals having the same stoichiometry: its Mg-analogue quintinite, $Mg_4Al_2(OH)_{12}CO_3 \cdot 3H_2O$, and its Fe^{2+}-analogue caresite, $Fe^{2+}{}_4Al_2(OH)_{12}CO_3 \cdot 3H_2O$. The work by Chao and Gault (1997) turned out to be pioneering in the approach to quintinite (and, consequently, quintinite-group minerals) that has been finally separated from hydrotalcite after 155 years during which two phases of different stoichiometry and properties took place under the same common name "hydrotalcite". Later studies showed a wider distribution of quintinite compared to hydrotalcite and fundamental structural differences between the two minerals especially with respect to the layer charge densities and associated properties (Wang et al., 2009; Mills *et al.*, 2016; Zhitova *et al.*, 2016, 2018).

Crystal structures of most LDHs remain unknown, owing to the absence of single crystals for synthetic materials and, as a result, the absence of starting crystal-structure models for the refinement of powder X-ray diffraction-data. In contrast, a number of structure models for synthetic LDHs have been studied on the basis of the investigations of their natural analogues (see summary in Mills *et al.*, 2012 and Zhitova *et al.*, 2019a).

To date, charmarite is an endemic mineral with unknown crystal structure. Charmarite is closely related to quintinite and caresite in terms of stoichiometry and, in general, chemistry. This prompts us to discuss these minerals together. In the work of Chao and Gault (1997) the unit-cell parameters of quintinite, caresite and charmarite have been determined by single-crystal photographic methods and refined by least-squares methods using X-ray powder-diffraction data (Table 1). Based on the single-crystal X-ray photographs Chao and Gault (1997) suggested the presence of $2\sqrt{3}a' \times 2\sqrt{3}a'$ (or $\sqrt{12}a' \times \sqrt{12}a'$) superstructure in all three minerals interpreted as ordering of di- and trivalent cations (Mills *et al.*, 2012). The first crystal structure determination of quintinite (Arakcheeva *et al.*, 1996) proposed the presence of the $\sqrt{3}a' \times \sqrt{3}a'$ superstructure (*a*' is further avoided in designation of superstructure) only due to the ordered arrangement of di- and trivalent cations. The systematic studies of crystal structures of quintinite from different worldwide localities indicated the existence of at least five polytypes differing for the presence or absence of the $\sqrt{3} \times \sqrt{3}$ Mg-Al ordering combined with different stacking sequences (Krivovichev *et al.*, 2010a,b; Zhitova *et al.*, 2010, 2018, 2023a) (Table 1). The

https://doi.org/10.1180/mgm.2024.11 Published online by Cambridge University Press

$2\sqrt{3} \times 2\sqrt{3}$ (or $\sqrt{12} \times \sqrt{12}$) structure was not determined and refined for any LDH (within almost 30 years after the first notice) and was considered questionable. Moreover, the crystal chemical mechanism of potential formation of the $2\sqrt{3} \times 2\sqrt{3}$ superstructure in LDHs remained unclear, since experimental observations has shown that the ordering of di- and trivalent cations (rather common for LDHs) do not result in such long-periodic (within *xy* plane) structures (e.g. Walenta 1984; Bonaccorsi *et al*., 2007). This attracted our attention to the crystal chemical investigation of charmarite, which is a subject of this work.

Materials

Charmarite studied in this work originates from the Mont Saint-Hilaire alkaline complex. The specimen was collected in 2004. The mineral occurs as hexagonal yellowish crystals and curved colourless hexagonal plates up to 0.05 mm in size (Fig. 1) chaotically grouped in clusters which overgrow dark-brown tabular laverovite crystal (1 cm × 1 cm in size) in association with white albite.

Methods

Chemical composition

The chemical analyses (5 points) were carried out with a Hitachi FlexSEM 1000 scanning electron microscope equipped with energy-dispersive spectrometry (EDS) Xplore Contact 30 detector and Oxford AZtecLive STD system of analysis. Analytical conditions were: accelerating voltage 15 kV, beam current 5 nA and beam size 2 μm. The standards used are given in Table 2.

Single-crystal X-ray diffraction

The single-crystal X-ray diffraction (SC XRD) data have been obtained from tabular hexagonal crystals of reddish colour. The experiment was carried out with Mo*K*α radiation by means of a Bruker Apex II Duo diffractometer (Bruker, Billerica, MA, USA) operated at 50 kV/1 mA and equipped with a charge coupled device (CCD) area detector.

The unit-cell check based on 250 reflections indicated the trigonal symmetry of the mineral (*P* cell) with $a = b = 10.97$, $c = 15.08$ Å. The full SC XRD data set was collected and separately processed using Bruker and CrysAlis software in automatic and manual (including check for twin domains) mode. The intensity data were reduced and corrected for Lorentz,

https://doi.org/10.1180/mgm.2024.11 Published online by Cambridge University Press

polarization, and background effects using CrysAlis PRO program (CrysAlis PRO, 2014). A semi-empirical absorption-correction based upon the intensities of equivalent reflections was applied (Bruker-AXS, 2014, Sheldrick, 2015). The unit-cell parameters were refined by the least-squares methods. Using Olex2 (Dolomanov et al., 2009), the structure was solved with the SHELXS (Sheldrick, 2008) structure solution program using direct methods and refined with the SHELXL (Sheldrick, 2015) refinement package using least squares minimization. The two-component twinning by matrix {-1 0 0 0 -1 0 0 0 1} was applied to the structure refinement. Crystal structures were visualized using the Vesta program (Momma, Izumi, 2011). All procedures resulted in the confirmation of aforementioned lattice. The topology of the obtained model was reasonable and the search for a higher symmetry by means of the Platon software (Spek, 2003) confirmed the correct choice of the space-group symmetry. We note that we have also obtained structure models in the space groups *P*3, *P*-3*m*1, *P*-62*m*, but none of these provided an improvement over the *P*-3 model. The alternative refinements in space group *P*-3*m*1 resulted in $R_1 = 0.1883$ based on 2222 unique observed reflections and without considerable structural difference and in the space group *P*-62*m* the refinement converged to $R_1 = 0.0827$ based on 2202 unique observed reflections with non-equivalent interlayers that seemed to us crystal chemically unreasonable.

Powder X-ray diffraction

Powder X-ray diffraction (XRD) data were collected from an intergrowth of lamellar charmarite crystals up to 0.2 mm in size using a Rigaku R-Axis Rapid II diffractometer (Debye-Scherrer geometry, $d = 127.4$ mm) equipped with a rotating anode X-ray source (Co$K\alpha$, $\lambda = 1.79021$ Å) and a curved image plate detector. The data were integrated using the software package Osc2Tab/SQRay (Britvin *et al.*, 2017) and processed using the International Centre for Diffraction Data (ICDD) database incorporated into PDXL program (Rigaku, 2018). The *h*, *k* and *l* values were calculated using the software package VESTA (Momma, Izumi, 2011) from the crystal structure model of charmarite obtained in this work. The unit-cell parameters of charmarite were refined by the Le Bail method implemented in Topas software (Bruker-AXS, 2009) using the starting structural model of charmarite reported therein. The refinement was based on the reflections in the 2θ region from 10 to 80°. The background was modelled by a Chebyshev polynomial approximation of the 12-th order, preferred orientation of the sample along the [002] direction was confirmed during the refinement.

Raman spectroscopy

https://doi.org/10.1180/mgm.2024.11 Published online by Cambridge University Press

The Raman spectrum of charmarite was obtained by Horiba Jobin-Yvon LabRam HR800 spectrometer, equipped with a solid-state laser (λ = 532 nm) at 50 mW output power and ~ 6 mW power at the sample surface for an area of 2 μm × 2 μm. The spectrum was recorded with resolution 2 cm^{-1} at room temperature from the plate previously used for powder X-ray diffraction data collection placed on a glass slide. The plate has been cleared of paratone oil (used for sample attachment in powder X-ray diffraction experiment), but some traces may remain. The spectrum was further processed using LabSpec (Horiba) software.

Results

Chemical composition

The chemical composition of charmarite in wt.% is given in Table 2. The empirical formula calculated on the basis of the sum of all metal cations = 6 *apfu* and OH = 12 *apfu* is: $(Mn_{3.94}Mg_{0.03}Fe_{0.01})_{\Sigma 3.98}Al_{2.01}(OH)_{12}CO_3 \cdot 3H_2O$. The CO_2 content has been calculated by charge balance. The OH and H_2O content has been calculated from stoichiometry of charmarite.

Single-crystal X-ray diffraction data

The data obtained for charmarite were indexed in the trigonal cell, space group *P*-3 with the following unit-cell parameters: $a = 10.9630(4)$, $c = 15.0732(5)$ Å and $V = 1568.89(12)$ $Å^3$. The correct choice of the unit cell is supported by the analysis of the reconstructed reciprocal space slices where regular superstructure reflections are clearly visible (Fig. 2). The crystal structure was solved and refined in the space group *P*-3 to $R_1 = 0.075$ for 3801 unique observed reflections with $F_o > 4\sigma(F_o)$ (Table 4). Atom coordinates, site occupancies and displacement parameters are given in Table 5. Selected bond lengths and angles are listed in Table 6, hydrogen bonding scheme is shown in Table 7. The anisotropic displacement parameters are given in Table S1. The crystallographic information file (cif) has been deposited (i) via the joint Cambridge Crystal Data Centre CCDC/FIZ Karlsruhe deposition service; the deposition number is CSD 2285202 and (ii) with the Principal Editor of *Mineralogical Magazine* and are available as Supplementary Material (see below).

Juxtaposition of the *hk*0 and 0*kl* reciprocal space sections is shown in Fig. 2e that outlines possible unit cells based on main and superstructure reflections and justify the choice of lattice with the $2\sqrt{3} \times 2\sqrt{3}$ (or $2\sqrt{3}a$`) supercell. The analysis of spots along *l* (stacking direction) shows that (i) two-layer hexagonal cell is well sustained (*k* = 0, 6); (ii) spots with *k* = 1, 3 are characterized by some diffuse scattering, but are clearly separated and assigned to the $2\sqrt{3} \times 2\sqrt{3}$

https://doi.org/10.1180/mgm.2024.11 Published online by Cambridge University Press

ordering along stacking direction; (iii) the strongest diffuse scattering is observed for the spots with $k = 2$ and 4 that mainly refer to the $\sqrt{3} \times \sqrt{3}$ superstructure. Possibly, the diffuse character of the spots with $k = 2$ and 4 reflects partial Mn-Al disorder in the octahedral sites the along stacking direction (with formation of mixed-occupied positions in some layers) as observed herein.

Powder X-ray diffraction data

Powder XRD data are provided in Table 3, the XRD pattern is presented in Fig. 3. The obtained powder XRD pattern of charmarite is very similar to that from the ICDD card #00-051-1529 (Chao and Gault, 1997), which corresponds to the original description of charmarite-2*H* (crystal structure undetermined, see comparison in Table 3). The polytype notation by Ramsdell (Ramsdell, 1947) is based on the number of layers within the unit cell and symmetry of the crystal structure. In LDHs there are two main types of layer stacking sequences: hexagonal that normally results in two-layer cells and rhombohedral that normally results in three-layer cells with symmetry reduction from trigonal to monoclinic one-layer cells being also rather widespread (Krivovichev et al., 2010; Zhitova et al., 2018). From powder X-ray diffraction data and preliminary single-crystal X-ray diffraction data the layer stacking sequence can be determined: hexagonal or rhombohedral that commonly interpreted as 2*H* and 3*T*/3*R* polytypes, respectively. However, the full symmetry of the crystal structure (*T*, *H*, *M*, etc.) can be affected by cation and/or anion ordering and requires detailed structure analysis. In the original work by Chao and Gault (1997) the polytypes for charmarite, caresite and quintinite were determined as 2*H* and 3*T*. This study shows (by the structure refinement using single-crystal X-ray diffraction data) cation and anion ordering for charmarite with the hexagonal layer stacking sequence resulting in trigonal cell and polytype notation as 2*T*. The difference in the suffix for polytype notation for charmarite used by Chao and Gault (1997) as 2*H* and this work as 2*T* is not due to any structure differences, but due to structure peculiarities revealed by single-crystal X-ray diffraction herein. The refined unit cell parameters of charmarite-2*T* from the powder X-ray diffraction data are as follows: $a = 10.9934(6)$, $c = 15.1426(11)$ Å and $V = 1584.9(2)$ Å^3.

For the easier comparison the lattice parameters obtained by different methods we have reduced them to the sublattice, i.e. the distance between the two nearest metal atoms (a`) and the distance between two octahedral layers ($d_{00n}$). The obtained values are $a` = a/2/\sqrt{3} = 3.17$ Å obtained by powder X-ray diffraction *versus* 3.16 Å obtained by single-crystal X-ray diffraction and $d_{00n} = c/2 = 7.57$ Å obtained by powder X-ray diffraction *versus* 7.54 Å obtained by single-crystal X-ray diffraction. The comparison shows that isomorphic substitution (influencing in-plane a` parameter) is negligible. The difference in the c parameter (d_{00n}) is larger, but also

https://doi.org/10.1180/mgm.2024.11 Published online by Cambridge University Press

insignificant for layered compounds and fluctuates around the value of 7.56 Å most often found in stoichiometric quintinite. In view of the insignificance of these changes in d_{00n}, it seems that they may be more likely associated with a change in the height of the octahedral layer due distortions of the octahedra, rather than the change in stoichiometry (variations in the M^{2+}:M^{3+} ratio), since the second factor usually causes more significant changes in the interlayer distance, but the height of the octahedral layer fluctuates within 0.0n Å (Zhitova et al., 2016). Finally, unit cell parameters determined by single-crystal and powder X-ray diffraction differ by ~ 1 % (due to multiplication of these small differences) that is in a good agreement, taking into account that different crystals of charmarite were studied by these diffraction techniques.

Raman spectroscopy

The Raman spectrum of charmarite-2*T* is shown in Fig. 4a,b and is compared with the Raman spectra of quintinite and caresite in Fig. 4 and Table 8. The spectrum contains bands of O–H stretching vibrations and symmetric C–O stretching vibrations that are in agreement with charmarite chemistry in terms of light elements (C, H) the determination of that is problematic by other methods. In general, Raman spectra of charmarite, quintinite and caresite are similar (Table 8) that confirms their structural and chemical similarity.

Discussion

The crystal structure of charmarite consists of two types of metal-hydroxide layers located at the levels z = 0 (type 1) and ½ (type 2) and two interlayers located at the levels of z = ¼ and ¾ (Fig. 5). Each metal-hydroxide layer consists of four metal sites *M*(1-4) for the octahedral sheet 1 and *M*(5-8) for the octahedral sheet 2 (Fig. 6). Each *M* site is octahedrally coordinated by OH groups. The $M(OH)_6$ octahedra are edge-shared to form brucite-type sheets.

The octahedral sheets of the type 2 are characterized by the contrasting occupancy of the *M* sites: the *M*(5) and *M*(6) sites are nearly fully occupied by Mn, while the *M*(7) and *M*(8) sites are almost completely occupied by Al. This agrees well to the average *M*–O distances and the polyhedral volumes of the respective octahedra: the Mn-occupied octahedra (both *M*(5)- and *M*(6)-centred) have the average *M*(5,6)–O distance of 2.18 Å (and polyhedral volumes of 12.8-12.9 Å^3), while the Al-centred octahedra have <*M*(7)–O> = 1.92 Å and <*M*(8)–O> = 1.90 Å (with polyhedral volumes equal to 9.3 and 9.1 Å^3, respectively). The Mn-centred octahedra exhibit significant angular distortion (Table 9) in order to fit to the lengths of shared edges with neighbouring small $Al(OH)_6$ (the shared edge of ~ 2.58 Å) octahedra and large $Mn(OH)_6$

https://doi.org/10.1180/mgm.2024.11 Published online by Cambridge University Press

octahedra (the shared edge of ~ 2.99 Å) (Fig. 6c). The geometry of the $Al(OH)_6$ octahedra seems to be unaffected by distortion (Table 9). The total occupancy of the *M*(5-8) sites agrees with charmarite ideal stoichiometry Mn_2Al with the small amount of a lighter cation, possibly Mg (total *epfu* 121(3) ē, while the ratio Mn:Al = 2:1 suggesting the ideal *epfu* value of 126 ē; see Table 5).

The octahedral sheets of the type 1 are characterized by the mixed occupancy of the *M*(1-4) sites: the *M*(1) and *M*(2) sites have higher number of electrons per formula unit (*epfu*) in comparison to the *M*(3) and *M*(4) sites. The occupancies agree well with the average *M*–O bond lengths: 2.12 Å for the *M*(1)- and *M*(2)-centred octahedra, 2.05 Å for the *M*(3)-centred octahedra, and 2.03 Å for the *M*(4)-centred octahedra. The general tendency is that the *M*(1) and *M*(2) octahedra are preferentially occupied by Mn, while the *M*(3) and *M*(4) octahedra are preferentially occupied by Al. The layer topology of the octahedral sheet of the type 1 agrees with the topology of the octahedral sheet 2 in position of Mn- and Al-centred octahedra, while occupancies of Mn- and Al-centred octahedra are different. The total occupancy of the *M*(1-4) sites is in agreement with the ideal charmarite stoichiometry Mn_2Al as 125(3) ē versus ideal value of 126 ē (Table 5).

The interlayers accommodate carbonate groups and H_2O molecules in-between the octahedral sheets. The $C(2)O_3$ carbonate groups concentrate in the trigonal prism formed by *M*(8) (*i.e.* Al) sites from the adjacent sheets, whereas the $C(1)O_3$ and $C(3)O_3$ carbonate groups are in the trigonal prisms formed by *M*(1) (Mn) and *M*(5) (Mn) sites from the adjacent sheets (Fig. 6b,d). The interaction between the interlayer $(CO_3)^{2-}$ anions and $(OH)^-$ groups of metal-hydroxide layers is realized through O–H···OCO_2 hydrogen bonds. The H atoms not involved in the bonding between OH groups and $(CO_3)^{2-}$ anions form hydrogen bonds to interlayer H_2O molecules (Fig. 5). Octahedral sheets are linked by weak hydrogen bonding to carbonate groups (O···O ~ 2.90 Å) and H_2O molecules (O···O ~ 2.6–2.8 Å). The general tendency in the localization of $(CO_3)^{2-}$ groups is that they do not occur in the neighbouring trigonal prisms of H atoms (Fig. 6b,d). There is some disorder associated with the carbonate and H_2O molecules in interlayers reflected by partial occupancies of the interlayer C and O sites. There are three C sites in the interlayer (Figs 5, 6), however in accord with charge requirements and taking into account two interlayers per unit-cell, only two $(CO_3)^{2-}$ groups are needed per one interlayer (per unit-cell mesh) to compensate the charge leading to some statistical disorder in their localization. The same is also true about the occupancy of interlayer O atoms some of which belong to $(CO_3)^{2-}$ groups, whereas the rest belongs to H_2O molecules. The local position of H_2O molecules is

https://doi.org/10.1180/mgm.2024.11 Published online by Cambridge University Press

sensible to localization of $(CO_3)^{2-}$ group and compensate spare bond strengths of metal-hydroxide layers.

The observed herein $2\sqrt{3} \times 2\sqrt{3}$ superstructure agrees with the arrangement of symmetrically independent Al sites [i.e. *M*(7) and *M*(8) in one sheet]. However, the differences in the geometry of symmetrically independent Al-occupied sites (measured by bond lengths and polyhedral distortions) is small (Table 9), which indicates that these differences are hardly responsible for the doubling of the *a* unit-cell parameter. The position of the interlayer components is more remarkable. The analysis of the localization of the $(CO_3)^{2-}$ anions shows that they are arranged according to the 2×2 superstructure (in which each second trigonal prism is empty) (Fig. 6b,d). At the same time Mn and Al atoms are arranged according to the $\sqrt{3} \times \sqrt{3}$ superstructure. The combination of these superstructures leads to the formation of the $2\sqrt{3} \times 2\sqrt{3}$ superstructure that allows ordering of both (i) Mn and Al cations in octahedral sheets and (ii) $(CO_3)^{2-}$ anions in the interlayers. The answer to the question on why then the $2\sqrt{3} \times 2\sqrt{3}$ superstructure has not been previously observed in carbonate and other LDHs may lay in the specific chemical composition of the mineral. According to the data on ionic radii (Shannon, 1976), six-coordinated Mn^{2+} cation has the radius of 0.81 Å (low spin) or 0.97 Å (high spin). In the crystal structure of charmarite, the *M*(5) site is occupied nearly exclusively by Mn with the *M*(5)–O distance of 2.18 Å. Taking into account the O^{2-} radius of 1.22 Å (Shannon, 1976), the *M*(5)–O distance corresponds to the ionic radius of high-spin Mn^{2+} ion (0.97 Å). The ionic radius of Al^{3+} is 0.675 Å, while Mg (dominant divalent cation in quintinite) has the crystal radius of 0.86 Å. So, the species-forming cations Mn^{2+} and Al in charmarite have more significant difference in the size than Mg and Al in quintinite. Hypothetically, this should lead to the higher tendency of Mn and Al to order as di- and trivalent cations. The higher degree of ordering of di- and trivalent cations within octahedral sheets is responsible for the ordering of interlayer components that follows the scheme of charge distribution. The general tendency revealed recently for Cl-dominant LDHs shows that higher degree of ordering of di- and trivalent cations leads to the higher degree of ordering of interlayer components that has been reflected by the occupancy of interlayer Cl and O (of H_2O) sites in chlormagaluminite and dritsite with the $\sqrt{3} \times \sqrt{3}$ superstructure *versus* iowaite that shows the 1×1 (disordered) unit cell (Zhitova *et al.*, 2019b,c; 2023b).

Perhaps, not the last role may be played by the possibility of detecting weak superstructure reflections and superstructures, which is influenced by such factors as the scattering power of atoms (which is more than twice higher for Mn than for Mg), the crystal quality, and the detector sensitivity. The previous studies of quintinite and chlormagalumite

https://doi.org/10.1180/mgm.2024.11 Published online by Cambridge University Press

(Zhitova *et al*., 2018, 2019b) were performed on the same diffractometer as the one used for the study of charmarite. Therefore, we believe that, among the listed factors, the technical reasons are the least ones.

Acknowledgements

This research was supported by the Russian Science Foundation (project no. 22-77-10036 for ESZ, AAZ and RMS). Technical support of the St. Petersburg State University Resource Centres "X-ray diffraction research methods" and "Geomodel" is carried out within the framework of SPbSU, grants No. AAAA-A19-119091190094 and No. 103752493, for both Resource Centres, respectively. We would like to thank the reviewers for constructive comments.

Competing interests: The authors declare none.

References

Andersen A.B.A., Henriksen C., Wang Q., Ravnsbæk D.B., Hansen L.P. and Nielsen U.G. (2021) Synthesis and thermal degradation of $MAl_4(OH)_{12}SO_4{\cdot}3H_2O$ with M = Co^{2+}, Ni^{2+}, Cu^{2+}, and Zn^{2+}. *Inorganic Chemistry*, **60**, 16700–16712.

Arakcheeva A.V., Pushcharovskii D.Y., Rastsvetaeva R.K., Atencio D. and Lubman G.U. (1996) Crystal structure and comparative crystal chemistry of $Al_2Mg_4(OH)_{12}(CO_3){\cdot}3H_2O$, a new mineral from the hydrotalcite-manasseite group. *Crystallography Reports*, **41**, 972–981.

Bonaccorsi E., Merlino S. and Orlandi P. (2007) Zincalstibite, a new mineral, and cualstibite: crystal chemical and structural relationships. *American Mineralogist*, **92**, 198–203.

Bosa G., Silva C., Brito B., Terzi C., Wypych F. and Nakagaki, S. (2023) Revisiting the synthesis of gibbsite, a precursor for Li/Al LDH synthesis and its use as a support for porphyrin immobilization. *Journal of the Brazilian Chemical Society*, doi: 10.21577/0103-5053.20230095.

Britvin S.N., Dolivo-Dobrovolsky D.V. and Krzhizhanovskaya M.G. (2017) Software for processing the X-ray powder diffraction data obtained from the curved image plate detector of Rigaku RAXIS Rapid II diffractometer. *Zapiski Rossiiskogo Mineralogicheskogo Obshchestva*, **146**, 104–107 [in Russian with English abstract].

Britto S. and Kamath P.V. (2011) Polytypism in the lithium–aluminum layered double hydroxides: The $[LiAl_2(OH)_6]^+$ Layer as a structural synthon. *Inorganic Chemistry*, **50**, 5619–5627.

https://doi.org/10.1180/mgm.2024.11 Published online by Cambridge University Press

Bruker AXS (2009) *Topas, version 4.2; General Profile and Structure Analysis Software for Powder Diffraction Data*. Bruker-AXS, Karlsruhe, Germany.

Bruker AXS (2014) APEX2; Version 2014.11-0; Bruker AXS: Madison, WI, USA.

Chao G.Y. and Gault R.A. (1997) Quintinite-2H, quintinite-3T, charmarite-2H, charmarite-3T and caresite-3T, a new group of carbonate minerals related to the hydrotalcite - manasseite group. *The Canadian Mineralogist*, **35**, 1541–1549.

CrysAlis, PRO (2014) Agilent Technologies Ltd.: Yarnton, UK.

Dolomanov O. V., Blake A. J., Champness N. R. and Schröder M. (2009) OLEX: new software for visualization and analysis of extended crystal structures. *Journal of applied crystallography*, **36(5)**, 1283-1284.

Evans D.G. and Slade R.C.T. (2005) Structural aspects of layered double hydroxides. Pp. 1–87.

Forano C., Hibino T., Leroux F. and Taviot-Guého C. (2006) Chapter 13.1 layered double hydroxides. Pp. 1021–1095.

Grand L.M., Palmer S.J. and Frost R.L. (2010) Synthesis and thermal stability of hydrotalcites containing manganese. *Journal of Thermal Analysis and Calorimetry*, **100**, 981–985.

Guilherme V.A., Cunha V.R.R., de Paula E., de Araujo D.R. and Constantino V.R.L. (2022) Anti-inflammatory and analgesic evaluation of a phytochemical intercalated into layered double hydroxide. *Pharmaceutics*, **14**, 934.

Karim A.V., Hassani A., Eghbali P. and Nidheesh P.V. (2022) Nanostructured modified layered double hydroxides (LDHs)-based catalysts: a review on synthesis, characterization, and applications in water remediation by advanced oxidation processes. *Current Opinion in Solid State and Materials Science*, **26**, 100965.

Karpenko V.Yu., Zhitova E.S., Pautov L.A., Agakhanov A.A., Siidra O.I., Krzhizhanovskaya M.G., Rassulov V.A. and Bocharov V.N. (2020) Akopovaite, $Li_2Al_4(OH)_{12}(CO_3)(H_2O)_3$, a new Li member of the hydrotalcite supergroup from Turkestan Range, Kyrgyzstan. *Mineralogical Magazine*, **84(2)**, 301-311.

https://doi.org/10.1180/mgm.2024.11 Published online by Cambridge University Press

Krivovichev S.V., Yakovenchuk V.N., Zhitova E.S., Zolotarev A.A., Pakhomovsky Y.A. and Ivanyuk G.Yu. (2010a) Crystal chemistry of natural layered double hydroxides. I. Quintinite 2*H*-3*c* from the Kovdor alkaline massif, Kola peninsula, Russia. *Mineralogical Magazine*, **74**, 821–832.

Krivovichev S.V., Yakovenchuk V.N., Zhitova E.S., Zolotarev A.A., Pakhomovsky Y.A. and Ivanyuk G.Yu. (2010b) Crystal chemistry of natural layered double hydroxides. 2. Quintinite-1*M*: first evidence of a monoclinic polytype in M^{2+}-M^{3+} layered double hydroxides. *Mineralogical Magazine*, **74**, 833–840.

Krivovichev S.V., Antonov A.A., Zhitova E.S., Zolotarev A.A., Krivovichev V.G. andYakovenchuk V.N. (2012) Quintinite-1M from the Bazhenov deposit (Middle Urals, Russia): crystal structure and properties. *Bulletin of St. Petersburg University*. Series 7: Geology, Geography, **2**, 3–10 [in Russian with English abstract].

Lafuente B., Downs R.T., Yang H., Stone N. (2015) The power of databases: the RRUFF project. Pp. 1-30 in: Highlights in Mineralogical Crystallography (T. Armbruster and R.M. Danisi, editors). W. De Gruyter, Berlin, Germany.

Mills S.J., Christy A.G., Génin J.-M.R., Kameda T. and Colombo F. (2012) Nomenclature of the hydrotalcite supergroup: natural layered double hydroxides. *Mineralogical Magazine*, **76**, 1289–1336.

Mills S.J., Christy A.G. and Schmitt R.T. (2016) The creation of neotypes for hydrotalcite. *Mineralogical Magazine*, **80**, 1023–1029.

Momma K. and Izumi F. (2011) VESTA 3 for three-dimensional visualization of crystal, volumetric and morphology data. *Journal of Applied Crystallography*, **44**, 1272–1276.

Ramsdell L.S. (1947) Studies on silicon carbide. *American Mineralogist*, **32(1-2)**, 64-82.

Rigaku (2018) PDXL: Integrated X-Ray Powder Diffraction Software, Version 2.8.4.0 (October 23, 2018). Tokyo, Japan.

Rives V. (2001) *Layered Double Hydroxides: Present and Future*. Nova Science Publishers: New York, NY, USA.

https://doi.org/10.1180/mgm.2024.11 Published online by Cambridge University Press

Robinson K., Gibbs G. V. and Ribbe P. H. (1971) Quadratic elongation: a quantitative measure of distortion in coordination polyhedra. *Science*, **172(3983)**, 567-570.

Serna C.J. (1982) Crystal-chemical study of layered $[Al_2Li(OH)_6]^+X^-\cdot nH_2O$. *Clays and Clay Minerals*, **30**, 180–184.

Shannon R.D. (1976) Revised effective ionic radii and systematic studies of interatomic distances in halides and chalcogenides. *Acta Crystallographica section A: crystal physics, diffraction, theoretical and general crystallography*, **32(5)**, 751-767.

Sheldrick G. M. (2008) A short history of SHELX. *Acta Crystallographica*. Sect. A, **64(1)**, 112-122.

Sheldrick G.M. (2015) Crystal structure refinement with SHELXL. *Acta Crystallographica* Sect. C, **71**, 3–8.

Sissoko I., Iyagba E.T., Sahai R. and Biloen P. (1985) Anion intercalation and exchange in $Al(OH)_3$ - derived compounds. *Journal of Solid State Chemistry*, **60**, 283–288.

Sotiles A.R. and Wypych F. (2019) Converting Mn/Al layered double hydroxide anion exchangers into cation exchangers by topotactic reactions using alkali metal sulfate solutions. *Chemical Communications*, **55**, 7824–7827.

Spek A.L.J. (2003) Single-crystal structure validation with the program PLATON. *Journal of applied crystallography*, **36(1)**, 7–13.

Theiss F., López A., Frost R.L. and Scholz R. (2015) Spectroscopic characterisation of the LDH mineral quintinite $Mg_4Al_2(OH)_{12}CO_3\cdot 3H_2O$. *Spectrochimica Acta Part A: Molecular and Biomolecular Spectroscopy*, **150**, 758–764.

Walenta K. (1984) Cualstibit, ein neues Sekundärmineral aus der Grube Clara im mittleren Schwarzwald (BRD). *Chemie der Erde*, **43**, 255–260.

Wang S.L., Liu C.H., Wang M.K., Chuang Y.H. and Chiang P.N. (2009) Arsenate adsorption by Mg/Al–NO_3 layered double hydroxides with varying the Mg/Al ratio. *Applied Clay Science*, **43(1)**, 79-85.

https://doi.org/10.1180/mgm.2024.11 Published online by Cambridge University Press

Xu M. and Wei M. (2018) Layered double hydroxide-based catalysts: recent advances in preparation, structure, and applications. *Advanced Functional Materials*, **28**, 1802943.

Zhitova E.S., Yakovenchuk V.N., Krivovichev S. V., Zolotarev A.A., Pakhomovsky Y.A. and Ivanyuk G.Yu. (2010) Crystal chemistry of natural layered double hydroxides. 3. The crystal structure of Mg,Al-disordered quintinite-2*H*. *Mineralogical Magazine*, **74**, 841–848.

Zhitova E.S., Krivovichev S.V., Pekov I.V., Yakovenchuk V.N. and Pakhomovsky Y.A. (2016) Correlation between the *d*-value and the M^{2+}:M^{3+} cation ratio in Mg–Al–CO_3 layered double hydroxides. *Applied Clay Science*, **130**, 2-11.

Zhitova E.S., Popov M.P., Krivovichev S. V., Zaitsev A.N. and Vlasenko N.S. (2017) Quintinite-1*M* from the Mariinsky deposit, Ural Emerald Mines, Central Urals, Russia. *Geology of Ore Deposits*, **59**, 745–751.

Zhitova E.S., Krivovichev S. V., Yakovenchuk V.N., Ivanyuk G.Yu., Pakhomovsky Y.A. and Mikhailova J.A. (2018) Crystal chemistry of natural layered double hydroxides: 4. Crystal structures and evolution of structural complexity of quintinite polytypes from the Kovdor alkaline-ultrabasic massif, Kola peninsula, Russia. *Mineralogical Magazine*, **82**, 329–346.

Zhitova E.S., Krivovichev S.V., Pekov I.V. and Greenwell H.C. (2019a) Crystal chemistry of natural layered double hydroxides. 5. Single-crystal structure refinement of hydrotalcite, $[Mg_6Al_2(OH)_{16}](CO_3)(H_2O)_4$. *Mineralogical Magazine*, **83(2)**, 269-280.

Zhitova E.S., Krivovichev S.V., Pekov I.V. and Yapaskurt V.O. (2019b) Crystal chemistry of chlormagaluminite, $Mg_4Al_2(OH)_{12}Cl_2(H_2O)_2$, a natural layered double hydroxide. *Minerals*, **9(4)**, 221.

Zhitova E.S., Pekov I.V., Chaikovskiy I.I., Chirkova E.P., Yapaskurt V.O., Bychkova, Y.V., Belakovsky D.I., Chukanov N.V., Zubkova N.V., Krivovichev S.V. and Bocharov, V. N. (2019c) Dritsite, $Li_2Al_4(OH)_{12}Cl_2{\cdot}3H_2O$, a new gibbsite-based hydrotalcite supergroup mineral. *Minerals*, **9(8)**, 492.

Zhitova E.S., Sheveleva R.M., Zolotarev A.A. and Krivovichev S. V. (2023a) The crystal structure of Mg–Al–CO_3 layered double hydroxide. *Crystals*, **13**, 839.

Zhitova E.S., Chukanov N.V., Pekov I.V., Zolotarev A.A., Shilovskikh V.V. and Bocharov V.N. (2023b) Crystal chemistry of iowaite, $Mg_6Fe^{III}_2(OH)_{16}Cl_2{\times}4H_2O$, a natural layered double hydroxide. *Applied Clay Science*, **243**, 107070.

https://doi.org/10.1180/mgm.2024.11 Published online by Cambridge University Press

https://rruff.info/Caresite, accessed on 15 July 2023.

Table 1. Unit-cell parameters of quintinite group minerals: charmarite, caresite and quintinite

Mineral	Charmarite		Quintinite		Caresite
$M^{2+}{}_4Al^{3+}{}_2(OH)_{12}CO_3 \cdot 3H_2O$					
M^{2+}	Mn		Mg		Fe
Polytype	2*H*	3*T*	2*H*	3*T*	3*T*
Space group	$P6_322$	$P3_112$ or $P3_212$	$P6_322$	$P3_112$ or $P3_212$	$P3_112$ or $P3_212$
a, Å	10.985(3)	10.985(3)	10.571(1)	10.558(2)	10.805(3)
c, Å	15.10(2)	22.63(3)	15.1139(7)	22.71(3)	22.48(3)
V, Å^3	1578(3)	2366(4)	1465(1)	2192(3)	2273(4)
Z	4	6	4	6	6
a`, Å[(1)]	3.17	3.17	3.05	3.05	3.12
d_{00n}, Å[(2)]	7.55 (×2)	7.54 (×3)	7.57 (×2)	7.57 (×3)	7.49 (×3)
Reference	Chao and Gault (1997)				
Mineral	Quintinite				
Polytype	3*R*	1*M*	2*H*	2*T*	2*T*-3*c*
Space group	*R*-3*m*	*C*2/*m*	$P6_3/mmc$	*P*-3*c*1	*R*32
a, Å	3.06	5.23–5.29	3.02–3.06	5.25–5.31	5.27
b, Å	= *a*	9.05–9.15	= *a*	= *a*	= *a*
c, Å	22.67	7.70–7.81	15.06–15.23	15.07–15.23	45.36
β, º	90	103.0–103.2	90	90	90
V, Å^3	184.2	356–367	120–124	360–371	1093.0
a`, Å	3.06	3.02-3.06	3.02–3.06	3.03–3.07	3.05
d_{00n}, Å	7.56	7.53–7.61	7.56–7.63	7.53–7.61	7.56
Reference	1	2,3,4,5	6	1	7

(1) *a*` is the distance between two neighbouring *M* cations;

(2) d_{00n} is the distance between two neighbouring octahedral sheets.

References: 1 – Zhitova *et al.*, 2018; 2 – Krivovichev *et al.*, 2010b, 2012; 3 – Zhitova *et al.*, 2017; 4 – Zhitova *et al.*, 2017; 5 – Krivovichev *et al.*, 2012 ; 6 – Zhitova *et al.*, 2010; 7 – Krivovichev *et al.*, 2010a.

https://doi.org/10.1180/mgm.2024.11 Published online by Cambridge University Press

Table 2. Chemical composition of charmarite.

Constituent	Wt.%	Range	Stand. Dev.	Standards
MgO	0.22	0.07–0.40	0.13	Mg_2SiO_4
MnO	46.98	46.69–47.43	0.32	Mn_2SiO_4
FeO	0.15	0.05–0.26	0.09	FeS_2
Al_2O_3	17.19	16.87–17.86	0.39	Kyanite
CO_2[(1)]	7.42			
H_2O[(2)]	27.25			
Total	**99.21**			

[(1)] calculated by charge balance;

[(2)] calculated from the ideal stoichiometry of charmarite.

https://doi.org/10.1180/mgm.2024.11 Published online by Cambridge University Press

Table 3. Powder X-ray diffraction data obtained for charmarite-2*T* compared to the original data for charmarite-2*H* provided by Chao and Gault (1997)

This work, charmarite-2*T*							Charmarite-2*H*, ICDD # 00-051-1529 Chao and Gault (1997)	
d_{obs} (Å)	d_{calc} (Å)	I_{obs} (%)	I_{calc} (%)	*h*	*k*	*l*	d_{meas} (Å)	I_{rel} (%)
7.56	**7.54**	**100**	**100**	**0**	**0**	**2**	**7.53**	**100**
3.782	**3.768**	**34**	**19**	**0**	**0**	**4**	**3.768**	**60**
2.747	2.741	14	5	2	2	0	2.743	10
2.702	2.696	9	3	2	2	1	2.702	10
	2.696		3	2	2	-1		
2.580	**2.576**	**20**	**9**	**2**	**2**	**2**	**2.578**	**50**
	2.576		**9**	**2**	**2**	**-2**		
2.409	2.406	12	3	2	2	3	2.410	10
	2.406		3	2	2	-3		
2.222	**2.216**	**21**	**8**	**2**	**2**	**4**	**2.221**	**40**
	2.216		**8**	**2**	**2**	**-4**		
2.034	2.028	8	2	2	2	5	2.031	10
	2.028		2	2	2	-5		
1.857	**1.852**	**23**	**7**	**2**	**2**	**6**	**1.856**	**40**
	1.852		**7**	**2**	**2**	**-6**		
1.587	1.582	7	7	6	0	0	1.585	20
1.557	1.553	10	3	2	2	8	1.552	40
	1.553		3	2	2	-8		
1.373	1.370	3	1	4	4	0	1.325	5
1.000	0.999	6	1	2	8	4	n.p.	n.p.
	0.999		1	2	8	-4	n.p.	n.p.
	0.999		1	8	2	4	n.p.	n.p.
	0.999		1	8	2	-4	n.p.	n.p.

n.p. – not provided by Chao and Gault (1997). The five strongest reflections are highlighted in bold type.

https://doi.org/10.1180/mgm.2024.11 Published online by Cambridge University Press

Table 4. Crystal data, data collection information and structure refinement details for charmarite-2*T*.

Crystal chemical data	
Crystal system	Trigonal
Space group	*P*-3
a (Å)	10.9630(4)
c (Å)	15. 0732(5)
V (Å^3)	1568.89(12)
Z*	4
Calculated density (g/cm^3)	2.370
Absorption coefficient	3.137
Crystal size, mm	0.1 × 0.1 × 0.05
Data collection	
Diffractometer	Bruker Apex II Duo
Temperature (K)	293(2)
Radiation, wavelength (Å)	Mo*K*α, 0.71073
Range of data collection, 2θ (°)	4.29 – 75.292
h, *k*, *l* ranges	-18→17, -15→17, -25→24
Total reflection collected	47865
Unique reflections (R_{int})	5171 (0.0415)
Number of unique reflections $F > 2\sigma(F)$	3801
Data completeness (%)	99.9
Structure refinement	
Refinement method	Full-matrix least-squares on F^2
Weighting coefficients a, b	0.1766, 2.7007
Data/ restrain/ parameters	5171/13/191
R_1 [$F > 2\sigma(F)$], wR_2 [$F > 2\sigma(F)$]	0.0750, 0.2800
R_1 all, wR_2 all	0.0961, 0.3040

https://doi.org/10.1180/mgm.2024.11 Published online by Cambridge University Press

Goodness-of-fit on F^2	1.053
Largest diff. peak and hole ($\bar{e}Å^{-3}$)	1.40/-1.25

* for the formula $Mn_{3.7}Al_{2.3}(OH)_{12}CO_3 \cdot 1.9H_2O$.

https://doi.org/10.1180/mgm.2024.11 Published online by Cambridge University Press

Table 5. Atom coordinates, equivalent isotropic displacement parameters (Å^2), site occupancies and assigned site populations for charmarite-2*T*.

Site	Atom	*x*	*y*	*z*	U_{eq}	s.o.f.	*epfu**
Octahedral sheet (type 1)							
***M*1**	**Mn1**	2/3	1/3	0.00966(13)	0.0197(5)	0.62(2)	125(3) ē, $Mn_8Al_4(OH)_{24}$
	Al1	2/3	1/3	0.00966(13)	0.0197(5)	0.38(2)	
***M*2**	**Mn2**	0.83274(8)	0.16619(8)	0.00148(8)	0.0145(3)	0.76(2)	
	Al2	0.83274(8)	0.16619(8)	0.00148(8)	0.0145(3)	0.24(2)	
***M*3**	**Mn3**	1	0	0	0.0171(7)	0.59(3)	
	Al3	1	0	0	0.0171(7)	0.41(3)	
***M*4**	**Mn4**	½	0	0	0.0115(3)	0.56(2)	
	Al4	½	0	0	0.0115(3)	0.44(2)	
O1	**O1**	0.6619(4)	0.4971(3)	-0.0643(2)	0.0259(7)	1	
H1	**H1**	0.664(8)	0.501(8)	-0.1290(13)	0.043	1	
O2	**O2**	0.6593(4)	0.1577(4)	0.0698(2)	0.0335(8)	1	
H2	**H2**	0.676(7)	0.192(6)	0.1315(18)	0.043	1	
O3	**O3**	0.9993(4)	0.1621(4)	-0.06725(19)	0.0287(8)	1	
H3	**H3**	0.992(8)	0.178(8)	-0.1309(16)	0.043	1	
O4	**O4**	0.6605(4)	-0.0004(3)	-0.06662(19)	0.0256(7)	1	
H4	**H4**	0.662(8)	-0.014(7)	-0.1317(15)	0.043	1	
Octahedral sheet (type 2)							
***M*5**	**Mn5**	2/3	1/3	-0.51019(10)	0.0156(3)	0.944(18)	121(3) ē, $(Mn_{7.7}Mg_{0.3})Al_{4.0}(OH)_{24}$
	Al5	2/3	1/3	-0.51019(10)	0.0156(3)	0.056(18)	
***M*6**	**Mn6**	0.83293(8)	0.16634(8)	-0.50189(5)	0.0122(2)	0.79(2)	
	Al6	0.83293(8)	0.16634(8)	-0.50189(5)	0.0122(2)	0.21(2)	

DOI: 10.1180/mgm.2024.11

***M*7**	**Al7**	½	0	-½	0.0128(5)	0.94(2)	
	Mn7	½	0	-½	0.0128(5)	0.06(2)	
***M*8**	**Al8**	1	0	-½	0.0365(18)	0.96(3)	
	Mn8	1	0	-½	0.0365(18)	0.04(3)	
O5	**O5**	0.8542(3)	0.5023(3)	-0.56955(18)	0.0175(5)	1	
H5	**H5**	0.846(2)	0.509(2)	-0.6349(8)	0.027	1	
O6	**O6**	0.6500(3)	0.0013(3)	-0.4342(2)	0.0193(6)	1	
H6	**H6**	0.679(6)	0.021(6)	-0.3719(16)	0.027	1	
O7	**O7**	0.5026(3)	0.1524(3)	-0.43631(18)	0.0172(5)	1	
H7	**H7**	0.500(7)	0.178(6)	-0.3740(18)	0.027	1	
O8	**O8**	0.9988(3)	0.1473(3)	-0.4338(2)	0.0179(6)	1	
H8	**H8**	0.998(5)	0.166(5)	-0.3699(13)	0.027	1	
Interlayer gallery							
C1	**C1**	2/3	1/3	-0.2507(5)	0.0163(14)	0.79(3)	26(1) ē, $^{**}C_{2.2(2)}$
C2	**C2**	1	0	-0.2502(10)	0.020(2)	0.59(3)	
C3	**C3**	2/3	1/3	0.2375(16)	0.028(6)	0.28(3)	
O9	**O9**	0.7009(6)	0.0344(5)	-0.2540(4)	0.0302(14)	0.67(2)	214(10) ē, $^{**}O_{13(2)}$
O10	**O10**	0.6374(15)	0.0062(11)	-0.2422(9)	0.027(3)	0.273(18)	
O11	**O11**	0.5454(4)	0.2192(4)	-0.2517(3)	0.0309(10)	0.786(15)	
O12	**O12**	0.9815(5)	0.1063(5)	-0.2540(4)	0.0305(12)	0.588(13)	
O13	**O13**	0.6472(14)	0.2056(14)	0.2418(11)	0.021(4)	0.172(11)	
O15	**O15**	0.7321(13)	-0.0027(13)	0.2428(11)	0.044(4)	0.279(15)	
O16	**O16**	0.6674(5)	0.0668(5)	0.2544(5)	0.0329(15)	0.569(15)	

**epfu* – electrons per formula unit; *epfu* for Mn_8Al_4 (as in ideal formula) is 126 ē. **Note: $[(CO_3)(H_2O)_{3.5}]_2$

https://doi.org/10.1180/mgm.2024.11 Published online by Cambridge University Press

Table 6. Selected bond distances in (Å) for charmarite-2*T*.

Atom	Atom	Bond distance	Atom	Atom	Bond distance
Octahedral sheet 1			**Octahedral sheet 2**		
*M*1	O2	2.092(4) × 3	*M*5	O7	2.201(3) × 3
*M*1	O1	2.136(3) × 3	*M*5	O5	2.156(3) × 3
<*M*1–O>		**2.114**	**<*M*5–O>**		**2.178**
*M*2	O2	2.123(4)	*M*6	O7	2.178(3)
*M*2	O1	2.118(3)	*M*6	O6	2.170(3)
*M*2	O4	2.123(3)	*M*6	O6	2.168(3)
*M*2	O4	2.107(3)	*M*6	O5	2.177(3)
*M*2	O3	2.119(3)	*M*6	O8	2.175(3)
*M*2	O3	2.103(4)	*M*6	O8	2.187(3)
<*M*2–O>		**2.116**	**<*M*6–O>**		**2.176**
*M*3	O3	2.049(4) × 6	*M*7	O7	1.915(3) × 2
<*M*3–O>		**2.049**	*M*7	O6	1.914(3) × 2
*M*4	O1	2.037(3) × 2			
*M*4	O2	2.031(4) × 2	*M*7	O5	1.922(3) × 2
*M*4	O4	2.028(3) × 2	**<*M*7–O>**		**1.917**
<*M*4–O>		**2.032**	*M*8	O8	1.905(3) × 6
			<*M*8–O>		**1.905**
Interlayer gallery					
C1	O11	1.292(3) × 3	C3	O13	1.309(13) × 3
C2	O12	1.280(5) × 3			

Table 7. Hydrogen bonding scheme for charmarite-2*T*.

D–H	*d*(**D**–H)	*d*(H···**A**)	<**DHA**	*d*(**D**···A)	**A**
O1–H1	0.976(19)	1.94(3)	161(6)	2.876(6)	O11
O2–H2	0.986(19)	1.71(3)	161(6)	2.662(16)	O13
O3–H3	0.984(19)	2.00(4)	146(6)	2.867(7)	O12
		1.93(3)	163(6)	2.881(16)	O15
O4–H4	0.993(19)	1.91(3)	159(6)	2.855(7)	O9
		1.72(3)	157(6)	2.664(13)	O10
O5–H5	0.994(12)	1.936(17)	148.7(19)	2.833(8)	O16
O6–H6	0.981(19)	1.79(2)	170(5)	2.761(6)	O9
		1.99(3)	152(5)	2.899(13)	O10
O7–H7	0.985(19)	1.90(3)	162(6)	2.856(6)	O11
O8–H8	0.984(16)	1.84(3)	150(3)	2.738(7)	O12

This is a 'preproof' accepted article for Mineralogical Magazine. This version may be subject to change during the production process.
DOI: 10.1180/mgm.2024.11

Table 8. Raman bands observed in the spectra of charmarite, caresite and quintinite and their assignment

Charmarite	Caresite	Quintinite	Band assignment
3457	3460	3485	O–H stretching vibrations
3120 sh	3120 sh	3334, 3078	
1062	1060	1062, 1046 sh	Symmetrical stretching vibrations of carbonate groups
935 w	939 w	973 w	Water librational modes
697 w	695 w	698	Bending mode of carbonate
535	545	559	Lattice modes, possibly M^{2+}–O–M^{2+} vibrations
463 w	480 w	484 w	Lattice modes
435 sh w	459 sh w	401, 367	Lattice modes, possibly $M\cdots$O stretching vibrations
286 w	286 w	308	Lattice modes
218 w	-	-	Lattice modes
143	-	-	Lattice modes
This work	RRUFF database ID: R120028 Lafuente et al., 2015	Theiss et al., 2015	Reference

Table 9. Some geometrical parameters for MO_6 octahedra and occupancies of M sites

Octahedra	<M–O>, Å	Site occupancy	Quadratic elongation	Bond angle variance, degree^2	Distortion index	Polyhedral volume, Å^3
$M1$	2.114	$Mn_{0.62}Al_{0.38}$	1.03	99	0.010	12.03
$M2$	2.116	$Mn_{0.76}Al_{0.24}$	1.03	93	0.003	12.07
$M3$	2.049	$Mn_{0.59}Al_{0.41}$	1.02	64	0	11.14
$M4$	2.032	$Mn_{0.56}Al_{0.44}$	1.02	61	0.001	10.87
$M5$	2.178	$Mn_{0.94}Al_{0.06}$	1.05	148	0.010	12.86
$M6$	2.176	$Mn_{0.79}Al_{0.21}$	1.05	147	0.002	12.82
$M7$	1.917	$Al_{0.94}Mn_{0.06}$	1.01	30	0.002	9.27
$M8$	1.905	$Al_{0.96}Mn_{0.04}$	1.01	28	0	9.09

Quadratic elongation, bond angle variance, distortion index and polyhedral volume were introduced by Robinson et al. (1971) and have been calculated using Vesta software (Momma, Izumi, 2011).

https://doi.org/10.1180/mgm.2024.11 Published online by Cambridge University Press

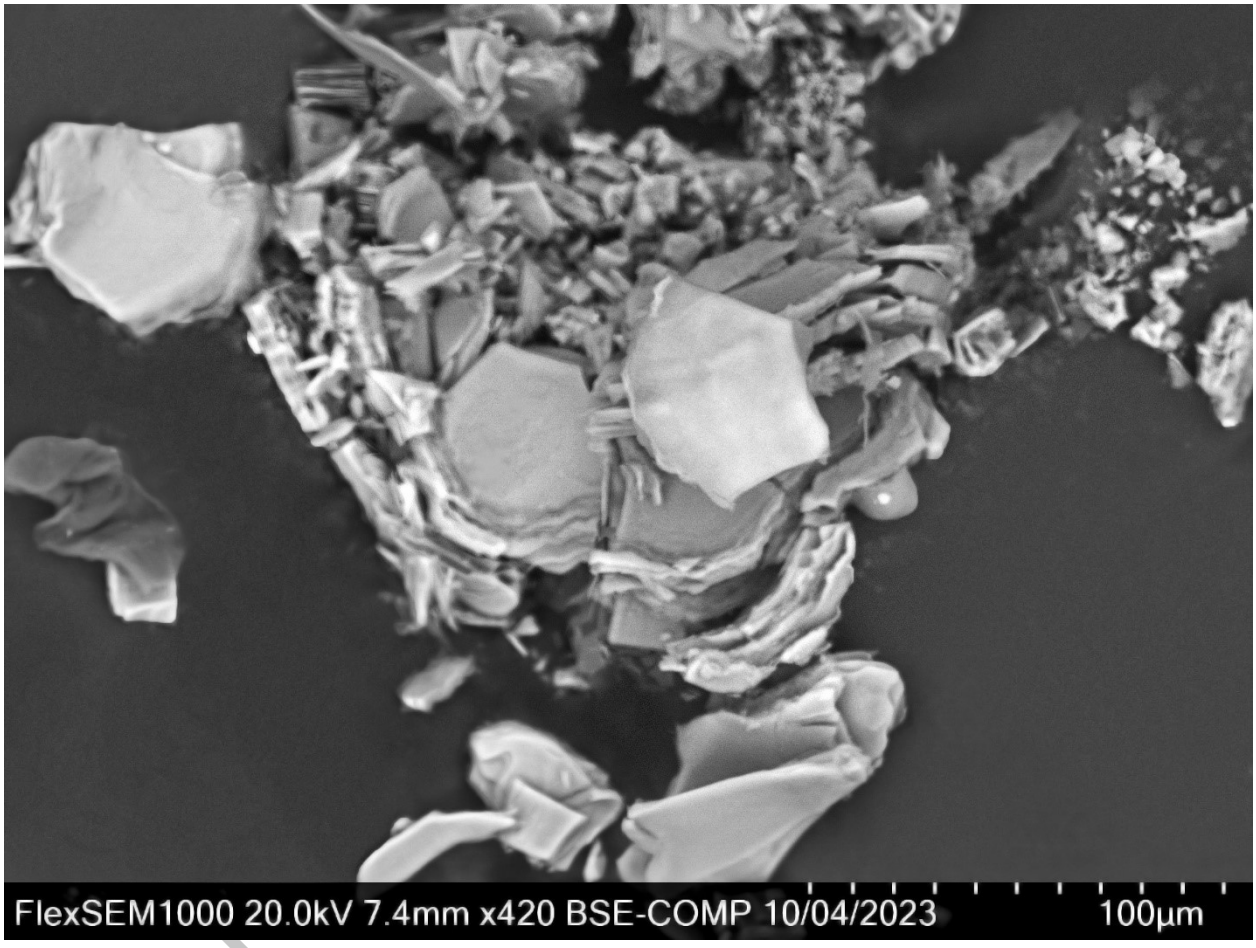

Fig. 1. Back-scattered electron image of a bunch of charmarite crystals.

https://doi.org/10.1180/mgm.2024.11 Published online by Cambridge University Press

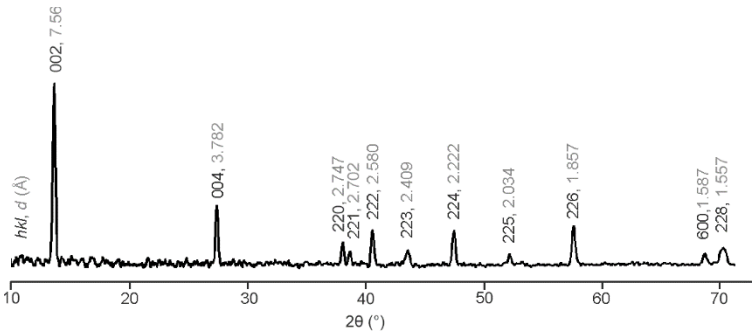

Fig. 2a-d. The reciprocal space slices of charmarite: (a) *hk*0 section, (b) *h*0*l* section, (c) enlarged part of *hk*0 section, indexed; (d) enlarged part of *h*0*l* section, indexed.

Fig. 2e. (e) juxtaposition of *hk*0 and 0*kl* sections.

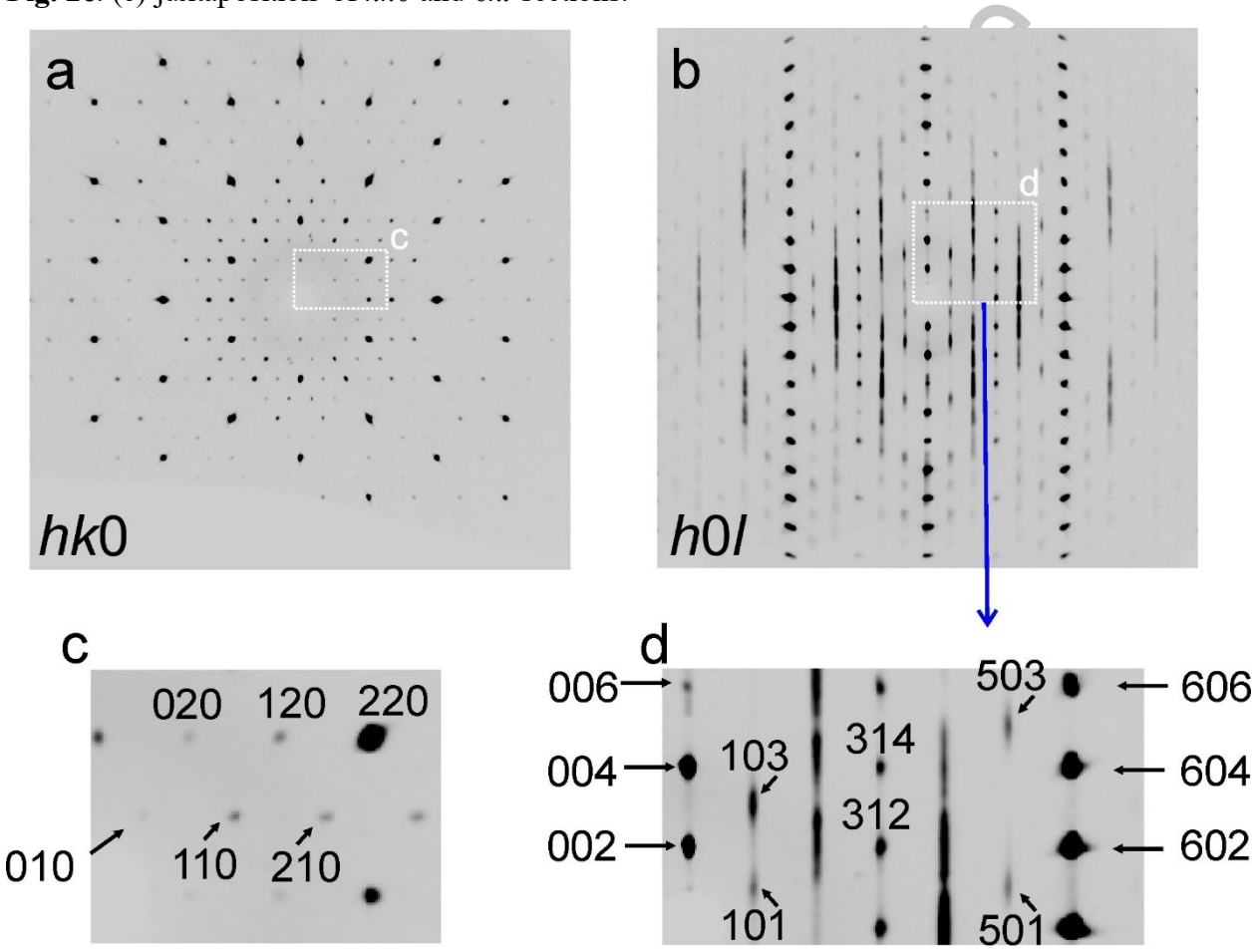

https://doi.org/10.1180/mgm.2024.11 Published online by Cambridge University Press

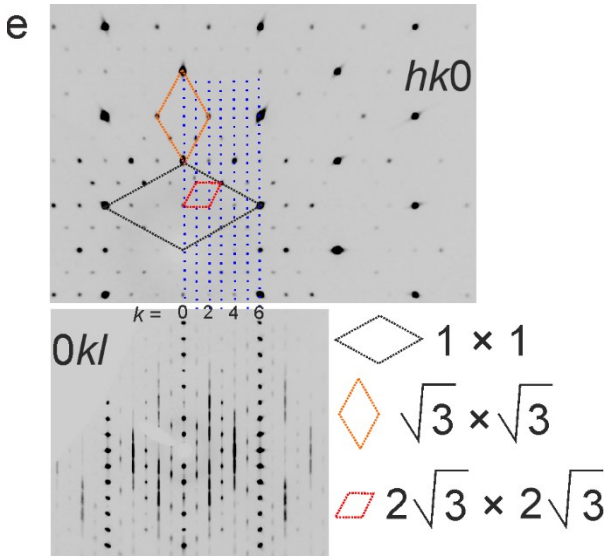

Fig. 3. Powder X-ray diffraction pattern of charmarite-2*T*.

https://doi.org/10.1180/mgm.2024.11 Published online by Cambridge University Press

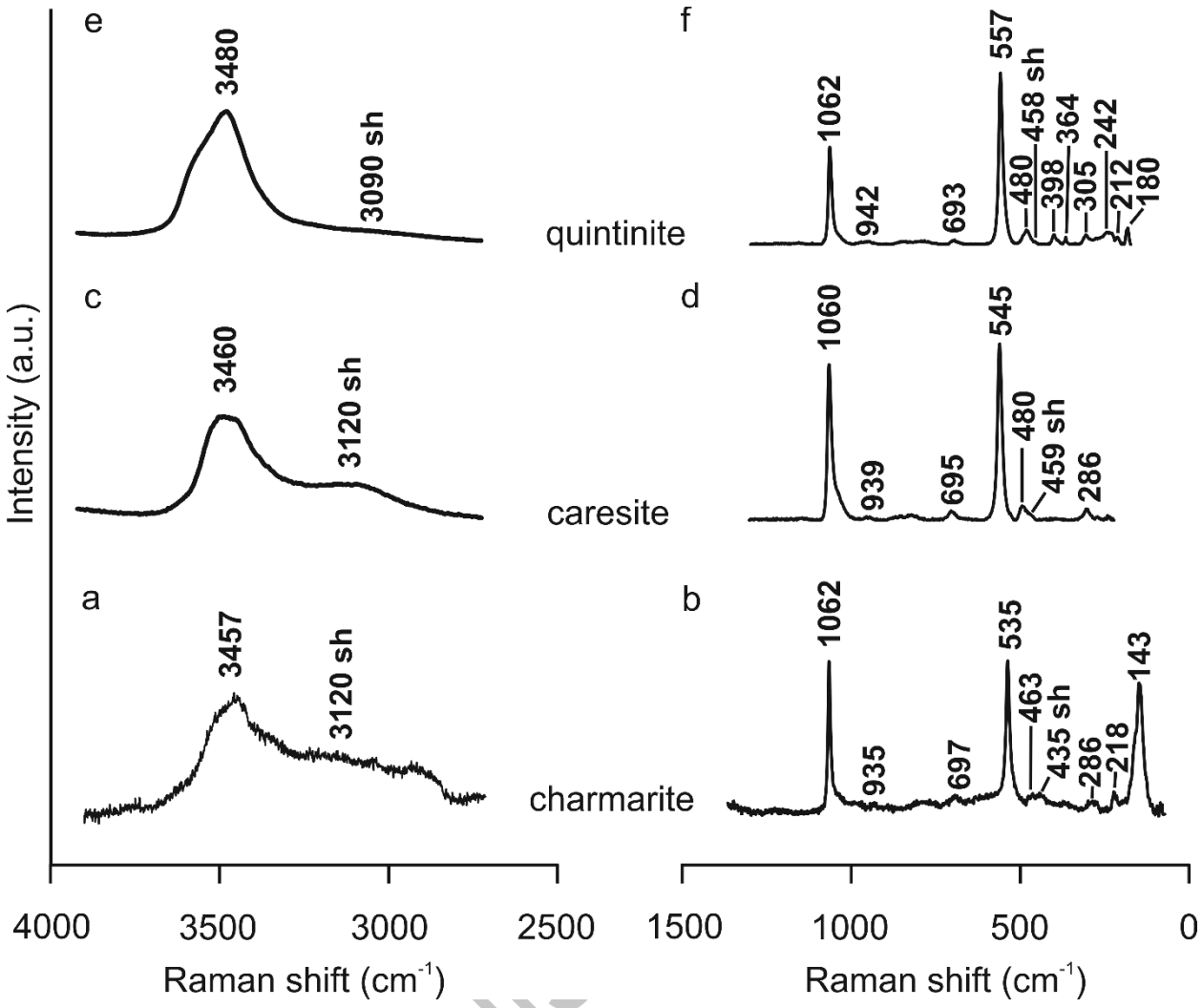

Fig. 4. Raman spectrum of charmarite obtained therein: (a) 4000 – 2500 cm^{-1} range and (b) 1500 – 0 cm^{-1} range compared to Raman spectra of caresite available in RRUFF database (under ID: R120028): (c) 4000 – 2500 cm^{-1} range and (d) 1500 – 0 cm^{-1} range and quintinite (e,f).

https://doi.org/10.1180/mgm.2024.11 Published online by Cambridge University Press

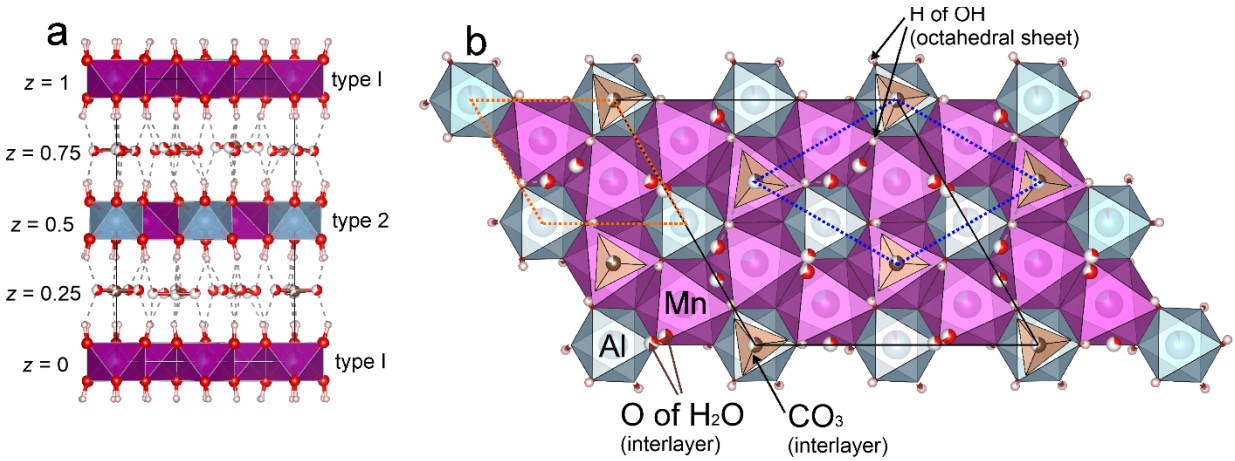

Fig. 5. The crystal structure of charmarite-2*T*: (a) projected perpendicular to the stacking direction and (b) within *xy* plane showing superstructure meshes [the unit-cell is outlined by solid black line; the 2 × 2 superstructure of interlayer carbonate groups (z = 0.75) is shown by blue dash; the $\sqrt{3} \times \sqrt{3}$ superstructure of M^{2+} and M^{3+} cations within octahedral sheet (z = 0.5) is outlined by orange dashed line] (see explanations in the text).

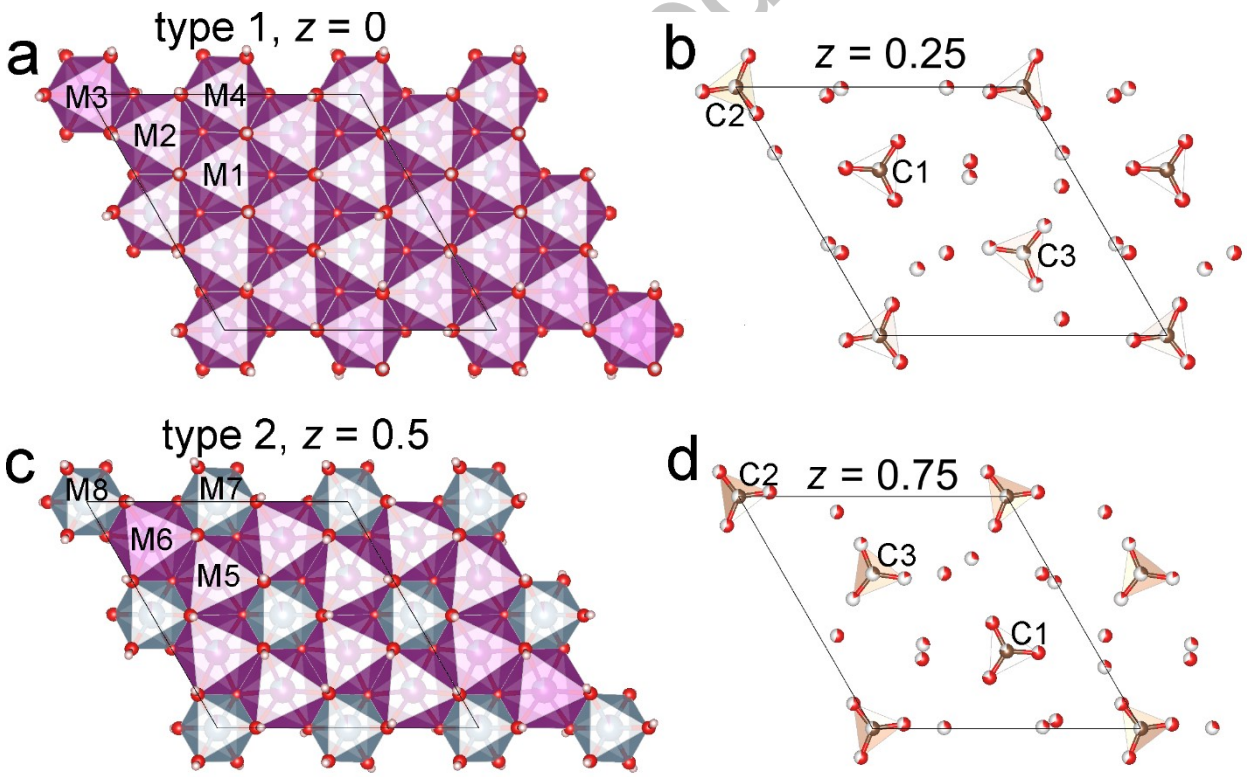

Fig. 6. The crystal structure of charmarite-2*T*: (a) octahedral sheet type 1, (b) interlayer at z = 1/4; (c) octahedral sheet type 2 and (d) interlayer at z = ¾.

https://doi.org/10.1180/mgm.2024.11 Published online by Cambridge University Press